KU LEUVEN

FACULTY OF SCIENCE
Department of Chemistry

A very cool Title:

An even cooler subtitle

DRAFT

To remove, add ‘final’ to class options

Mauro Gascón Navas

Dissertation presented in partial fulfillment
of the requirements for the degree of
Erasmus Mundus Master of Science in
Theoretical Chemistry and Computational
Modelling

Supervisors:
Prof. Dr. Thomas Jagau
Prof. dr. ir. S. Leader

June 2025

A VERY COOL TITLE:

AN EVEN COOLER SUBTITLE

Mauro GASCÓN NAVAS

Supervisors:
Prof. Dr. Thomas Jagau
Prof. dr. ir. S. Leader

Members of the
Examination Committee:
Prof. dr. ir. The Chairman, chair
Prof. dr. ir. The One
Prof. dr. ir. The Other
Prof. dr. External Jurymember
(Far Away)

Dissertation presented in partial fulfillment of the requirements for the degree of Erasmus Mundus Master of Science in Theoretical Chemistry and Computational Modelling

June 2025

Uitgegeven in eigen beheer, Mauro Gascón Navas, Leuven (Belgium)

Acknowledgements

. . .

Thank you thank you.

Instructions by the Arenberg Doctoral School:

The scientific abstract should present the most important aims and conclusions of the dissertation in a brief text of ca. 2 pages.

Abstract

...

Instructions by the Arenberg Doctoral School:

The scientific abstract should present the most important aims and conclusions of the dissertation in a brief text of ca. 2 pages.

Beknopte samenvatting

. . . aaa

Instructions by the Arenberg Doctoral School:

The scientific abstract should present the most important aims and conclusions of the dissertation in a brief text of ca. 2 pages.

List of Abbreviations

MD molecular dynamics. 11

List of Symbols

Θ	A nice symbol

Contents

List of Figures

List of Tables

Instructions by the Arenberg Doctoral School:

Report and discussion of the research in different chapters: These chapters, reporting and discussing research results, can be based on text that has already been published or accepted or submitted to journals or conferences. In that case, the bibliographic reference of the publication should be mentioned on the first page of the chapter. If there are multiple authors, the PhD researcher must clarify the own scientific contribution after that bibliographic reference on the first page of the chapter. There is no problem in editing or rewriting a text that has already been published or accepted for publication, for example to reach consistency and coherence in writing style and formatting, to add details that were left out from publication, to meet comments of the Examination Committee, etc; The doctoral candidate must determine whether the publisher allows public availability of the publications and in which form via the webpage Romeo/Sherpa.

Consistency in layout is required for the entire manuscript! References to figures, tables, appendices, and similar structures need to be consistent.

Chapter 1

Introduction

1.1 Electronic Processes in Biological Systems

Electrons are at the heart of all biochemical processes. From the generation of energy to the synthesis of biomolecules, the movement and distribution of electrons govern the reactivity and function of biological systems. Many key biological reactions are, at their core, charge transfer processes—redox reactions where electrons are transferred from one molecule to another. These reactions are often catalyzed by enzymes, which provide the appropriate environment to facilitate electron movement, stabilize intermediates, and control reaction kinetics with remarkable specificity and efficiency.

One of the most prominent examples of biological electron transfer is the respiratory chain in mitochondria. In this complex pathway, electrons derived from metabolic substrates are transferred through a series of protein complexes and mobile carriers, such as cytochromes and quinones, ultimately reducing molecular oxygen to water. In the process, a proton gradient is generated across the inner mitochondrial membrane, driving ATP synthesis via chemiosmotic coupling. Quinones, in particular, play a central role as redox-active cofactors that shuttle electrons and protons, and their ability to stabilize semiquinone and anionic states is essential to their function.

Another striking example is oxygenic photosynthesis, carried out by plants, algae, and cyanobacteria. Light energy is captured by pigment-protein complexes and used to drive electron transfer through the photosynthetic electron transport chain. This process begins with the photoexcitation of chlorophyll in photosystem II and ultimately leads to the reduction of $NADP^+$

to NADPH, with the concomitant generation of oxygen from water. The light-induced charge separation and subsequent electron transfer involve multiple cofactors, including chlorophylls, pheophytins, plastoquinones, and iron-sulfur clusters.

A third biological process involving complex electron dynamics is nitrogen fixation, carried out by nitrogenase enzymes in certain bacteria and archaea. Nitrogenase catalyzes the reduction of atmospheric nitrogen (N_2) to ammonia (NH_3), a reaction that requires the delivery of multiple electrons and protons. The enzyme contains a unique metallocluster cofactor (the FeMo-cofactor) that acts as a redox-active site for electron accumulation and N_2 activation. The electron flow is tightly regulated and coupled to ATP hydrolysis, and the mechanistic details of electron transfer and substrate binding remain areas of active research.

These examples illustrate the importance of electrons not just as abstract entities in chemical equations but as physical particles whose location, energy, and interactions must be understood to grasp biological function. Moreover, the existence of short-lived or weakly bound electronic states—such as nonvalence anions—can influence the dynamics of charge transfer processes, radical formation, and enzymatic activity. Understanding these transient electronic states requires experimental and computational tools capable of resolving both structure and electronic behavior on ultrafast timescales.

1.1.1 Experimental Approaches for Characterizing Electron Transfer

Studying such intricate electron-driven processes in biological systems is a challenging task that requires the integration of various experimental techniques. Traditionally, much of our understanding of enzymatic structure and function has come from structural biology. Techniques such as X-ray crystallography, nuclear magnetic resonance (NMR) spectroscopy, and cryo-electron microscopy (cryo-EM) allow researchers to determine the three-dimensional structures of proteins and complexes at atomic resolution. These structures are often deposited in public databases such as the Protein Data Bank (PDB), which provide critical starting points for further analysis.

Beyond static structures, insights into reaction mechanisms and kinetics are obtained through various spectroscopic methods. Ultraviolet-visible (UV-Vis) and infrared (IR) spectroscopy monitor changes in chromophores or functional groups during a reaction, while electron paramagnetic resonance (EPR) and Mössbauer spectroscopy provide information about unpaired electrons and

metal centers. Time-resolved spectroscopy, including pump-probe and transient absorption techniques, captures short-lived intermediates in electron transfer processes, revealing their lifetimes and dynamics.

Mass spectrometry has also become a powerful tool in the analysis of biomolecular reactions. It can be used to identify reaction products, post-translational modifications, or radical intermediates with high sensitivity. However, while these experimental approaches provide indispensable data, they often capture only fragments of the complete picture. For example, spectroscopy may detect the presence of a transient intermediate without resolving its precise structure or the detailed path of electron movement between donor and acceptor. Similarly, crystallographic data can sometimes miss critical information—such as the position of hydrogen atoms, associated water networks, or dynamic conformational states—that is essential for understanding electron transfer.

1.1.2 Modeling myBiological Electron Dynamics

Given the limitations of experimental techniques in capturing the full complexity of electron transfer in biology, computational modeling has become an indispensable tool. Starting from experimentally resolved structures from the PDB, researchers apply various theoretical methods to simulate and predict biological behavior across multiple scales.

At the macroscopic level, coarse-grained models and network-based approaches can describe signaling pathways, metabolic fluxes, or cellular dynamics. On the molecular scale, molecular dynamics (MD) simulations are widely used to explore the conformational flexibility of proteins and nucleic acids over time. MD simulations model atoms as classical particles interacting via empirical force fields, allowing the exploration of structural fluctuations, binding events, and diffusion processes. Such simulations provide valuable insight into the dynamic context within which electron transfer occurs.

Recent advances in machine learning have had a profound impact on structural biology. Tools like AlphaFold have dramatically improved our ability to predict protein structures directly from amino acid sequences. Although these models rely on statistical learning methods rather than directly solving physical equations, they generate highly accurate structures that serve as vital starting points for further investigations into electronic properties.

To directly study electron transfer and electron dynamics, quantum mechanical (QM) methods are required. Approaches such as Hartree–Fock theory, density functional theory (DFT), and post-Hartree–Fock methods (e.g., coupled-cluster theory) solve or approximate solutions to the Schrödinger equation, treating

electrons explicitly. These techniques reveal detailed information about chemical bonding, charge distribution, and reaction energetics. Despite their high accuracy, the computational cost of QM methods restricts their use to relatively small regions of a larger biological system, such as an enzyme active site or a cofactor.

Hybrid methods, notably quantum mechanics/molecular mechanics (QM/MM) simulations, provide a balance between accuracy and computational feasibility. In these methods, the region of primary interest—where electron transfer occurs—is treated using QM, while the surrounding environment is modeled using classical force fields. This allows a more realistic description of enzymatic reactions, electron transfer events, and proton-coupled mechanisms.

For elusive phenomena like nonvalence anionic states, even more sophisticated methods may be required. Such states, often weakly bound and highly sensitive to the surrounding electrostatic environment, may need advanced techniques that can capture long-range electron correlation and diffuse orbital characteristics. Methods such as equation-of-motion coupled-cluster theory (EOM-CC), Green's function approaches, and electron scattering calculations are sometimes employed to provide accurate descriptions of these transient states. Although these approaches come with significant computational cost, they are essential for uncovering the subtle electronic behavior that underpins key biological functions.

In summary, the integration of multiple modeling techniques—from coarse-grained methods to high-accuracy quantum approaches—enables a multiscale understanding of electron dynamics in biology. This holistic computational framework is crucial for elucidating the mechanisms of electron transfer and the roles played by nonvalence anions in biological systems, ultimately contributing to the broader understanding of enzymatic activity and energy conversion in living organisms.

Molecular anions are species in which a molecule possesses an extra electron, resulting in a negative charge. These systems are pervasive both in the gas phase and in biological environments. In many cases, molecular anions exhibit unusual stability, often persisting on timescales long enough to be isolated or characterized spectroscopically. Nonetheless, they are frequently transient intermediates, acting as precursors or doorway states that lead to further chemical transformations. Their behavior is intricately connected to factors such as molecular geometry, the environment (e.g., solvation or crystal lattice effects), and the energetic characteristics of the extra electron.

1.2 Molecular Anions and Their Role in Chemical Processes

The existence and behavior of molecular anions have been subjects of intense research because they encapsulate the interaction of excess electrons with molecular frameworks. In the gas phase, where perturbations from the environment are minimized, detailed studies have revealed long-lived anionic states that provide insight into intrinsic electron binding energies and the relaxation pathways following electron attachment. In contrast, within biological systems, the local environment, including solvent molecules and protein matrices, plays a significant role in stabilizing or destabilizing these excess electrons. This stabilization can lead to altered reactivities and modified pathways for both electron capture and subsequent chemical reactions.

1.2.1 Nonvalence Anions: Diffuse Electronic States and Electron Capture

Nonvalence anions represent a class of molecular anions where the extra electron occupies a diffuse orbital that is spatially decoupled from the usual valence orbitals of the molecule. This field, which emerged prominently among quantum chemists in the 1970s, has significantly advanced our understanding of electron localization in weak binding regimes.

Characteristics and Formation

In nonvalence anions, the additional electron is loosely attached, often residing in a highly diffuse orbital that extends well beyond the molecular skeleton. This leads to unique electronic states that differ markedly from those derived from traditional valence shell configurations. Because of the weak binding, nonvalence anions are extremely sensitive to external electric fields and the dielectric properties of their surroundings.

Role as Doorway States

One of the most exciting aspects of nonvalence anions is their role as doorway states for electron capture processes. In many reactions, particularly those involving biological macromolecules, these states can serve as transient intermediates that facilitate the capture and eventual stabilization of electrons. An exemplar of this behavior is the solvated electron in water, where a nearly free

electron is stabilized by a network of polar molecules. The interplay between nonvalence and valence electronic states in these systems can significantly influence reaction pathways and energy transfer processes.

1.2.2 Dipole Anions: Formation, Stability, and Experimental Debate

Dipole-bound anions are a subset of molecular anions that rely on the permanent dipole moment of a molecule for electron stabilization. When a molecule exhibits a sufficiently large dipole moment—typically exceeding a critical threshold that depends on the molecular structure and polarizability—the electrostatic potential can capture an excess electron in a diffuse orbital[6].

Critical Dipole Moment and Formation Criteria

The formation of a dipole-bound anion depends critically on the magnitude of the molecular dipole moment. Theoretical models predict that once the dipole moment surpasses a certain critical value (generally in the range of 2.5 to 2.8 Debye), the electron is capable of being bound in a diffuse orbital. Experimental investigations in the gas phase have confirmed the formation of dipole-bound states for a variety of molecules, revealing subtle dependencies on molecular geometry and polarizability.

Stability and Relevance in Different Phases

Despite their apparent stability in isolated gas-phase experiments, dipole-bound anions are often very short-lived species. Their transient nature arises due to the weak binding energy of the extra electron, making these states highly susceptible to perturbations such as collisions or solvation effects. While extensive studies have been conducted in the gas phase, the existence and stability of dipole-bound anions in solvated or biological environments remain topics of ongoing debate. In polar solvents, the competition between solvation stabilization and charge delocalization leads to complex behavior, and the experimental evidence for dipole-bound states in such systems is not always consistent.

1.2.3 Conclusion

In summary, molecular anions—encompassing both nonvalence and dipole-bound varieties—serve as key intermediates and transient states in a range of chemical

and biological processes. Their unique electronic structures and sensitivities to their environments not only challenge our understanding of electron-molecule interactions but also provide critical insights into the mechanisms underlying electron capture and transfer. Continuing research in this field is essential for advancing our knowledge of fundamental chemical processes, with implications spanning from atmospheric chemistry to biological electron transfer and beyond.

1.3 Electrons in Biology

. . . Explain reactions in biology, charge transfer reaction... Electrons are essential. Most reactions are conducted by enzymes... Some importnat pathways as respiratory chain (mention quinones), photosinthesis, nitrogenase...

1.3.1 How do We Get Knowledge About these systems?

How do we study enzymes... Protein crystalography, NMR etc... Structures are stored in the PDB... Can study by kinetics reactions by spectroscopy, mass spectroscopy... But experimental methods cannot ptovide the complete picture by themselves. . .

1.3.2 How do we model biology

Starting from the structures from the PDB, meny methods have been developed MD, AI (AlphaFold), QM... Each method seerves to provide a different view of the problem (kynetics, structure, thermodynamics...). Each method treats a different scale at different costs and accuracies... To model electron and electron dynamics we need high accuracy and costly methods...

1.4 Molecular Anions

Explain what is a molecular anion, how they exist in gas phase and in biology. They long lived times. They are usually transient species in time leading to other products. . . .

1.4.1 Nonvalence Anions

A field developed by quantum chemists from the 70s, the electron resides in a diffuse orbital. They are low energy lying stes that are very interesting when convined with a valence anion stat. They can act as doorway state to electron capture... Types of nonvalence anions. Examples of importnat systems as the solvated electron in water. ...

1.4.2 Dipole Anions

...Explain dipole bond anions. Critical dipole moments, again explain they are shortlived species. They have been studied in the gas phase extensively and there is debate on their existance in solvated systems.

1.5 Do Non-valence Anions Play a Critical Role in Biology?

Extensive wotk related to radiation damaga to the DNA as well as investigation on radiosesitizers... However little has been done in trying to asses their role in natural pathways. They could provide an elegant way to regulate long range electron transfer. A reason for its little investigation is the high cost of the needed methods to study them (CCSD, CASSCF...), and the little overlap between the research fields of the fields involved... This work aims to bridge this gap... ...

1.5.1 Biological Quinones

Quinones are a class of molecules that are everywhere in biology... they are essential to electron transfer pathways such as the respitatory chain and photosinthesis., They act as electron carriers between different enzimes... Coenzyme Q is one of the most common quinone... It presents a very interesting structure to study the role of nonvalence anions as it suports both a valence anion and dipole anion... It is possible that these states are not useful as they are very widespread but we want to asses the feasibility of their existance... ...

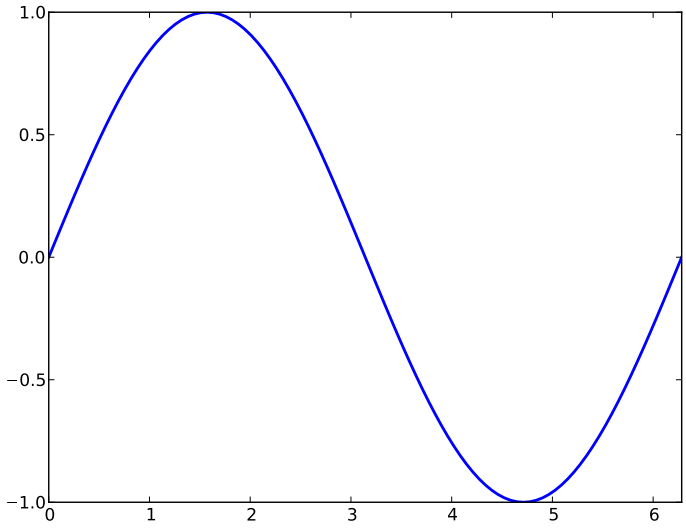

Figure 1.1: Illustration of how to include a figure (long text, should not go to Table of Figures).

1.6 Remove from here on

Introducing some symbol: Θ.

Introducing an acronym: MD.

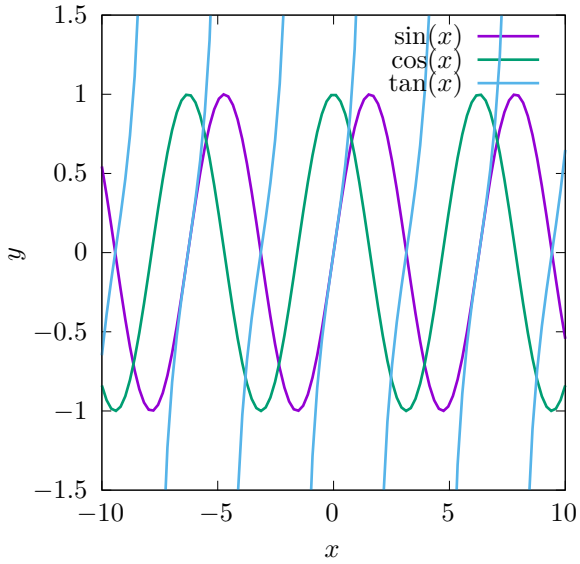

Figure 1.2: Illustration of how to include a figure (long text, should not go to Table of Figures).

Chapter 2

Theoretical Background

2.1 Self Consistent Field Methods

The objective of any quantum chemical calculation is to solve the time-independent Schrödinger equation (TISE) for a many-electron system:

$$\hat{H}\Psi = E\Psi \tag{2.1}$$

However, solving the TISE exactly for systems with more than one electron is computationally infeasible due to the complexity of electron-electron interactions. To address this, approximate methods such as the Hartree-Fock (HF) method have been developed[9].

The Hartree-Fock (HF) method stands as the cornestone electronic structure calculations. Its primary objective is to provide an approximate solution to the many-electron time-independent Schrödinger equation within the Born-Openhaimer approximation, which governs the behavior of electrons within atoms and molecules: The HF method achieves this by assuming that each electron moves independently within an average electrostatic field generated by the other electrons in the system. In the HF method the N-electron wavefunction is represented by a Slater determinant, which is formed by taking the antisymmetrized product of N individual one-electron spin-orbitals (χ):

$$\Psi(\mathbf{r}_1, \mathbf{r}_2, \ldots, \mathbf{r}_N) = \frac{1}{\sqrt{N!}} \begin{vmatrix} \chi_1(\mathbf{r}_1) & \chi_2(\mathbf{r}_1) & \cdots & \chi_N(\mathbf{r}_1) \\ \chi_1(\mathbf{r}_2) & \chi_2(\mathbf{r}_2) & \cdots & \chi_N(\mathbf{r}_2) \\ \vdots & \vdots & \ddots & \vdots \\ \chi_1(\mathbf{r}_N) & \chi_2(\mathbf{r}_N) & \cdots & \chi_N(\mathbf{r}_N) \end{vmatrix} \tag{2.2}$$

The choice of using a deteminant inherently satisfies both the Pauli exclusion principle, and the antisymmetry requirement of fermions. The energy expectation for a Slater determinant according to HF is variational and can be computed as:

$$\begin{aligned} E_{HF} &= \langle\Psi|\sum_{i=1}^{N}\hat{F}_i|\Psi\rangle \\ &= \langle\Psi|\sum_{i=1}^{N}\hat{h}(i) + \sum_{i,j=1}^{N}(2\hat{J}_j(i) - \hat{K}_j(i))|\Psi\rangle \\ &= \sum_{i=1}^{N}\langle\chi_i|\hat{h}|\chi_i\rangle + \frac{1}{2}\sum_{i,j=1}^{N}\langle\chi_i\chi_j||\chi_i\chi_j\rangle \end{aligned} \tag{2.3}$$

Where, $\hat{F}$ is the Fock operator. $\hat{F}$ is made up from $\hat{h}$, the one-electron core Hamiltonian operator (kinetic energy and electron-nucleus attraction); $\hat{J}_j(i)$, the Coulomb operator, describing the electrostatic repulsion between electron i and the average charge distribution of electron j, and $\hat{K}_j(i)$ is the exchange operator, a purely quantum mechanical term arising from the antisymmetry principle. Because of the two electron terms, the computational cost of HF scales as $O(N^4)$.

The Hartree-Fock equations are inherently non-linear: because the Fock operator depends on the wavefunctions of all the other electrons, their interactions are coupled. Consequently, these equations cannot be solved analytically and are solved using an iterative procedure known as the self-consistent field (SCF) method, where the final field experienced by the electrons must be consistent with the electron distribution that generates that field. The SCF procedure involves the following steps: An initial guess for the spin-orbitals is made. Using this initial guess, the Fock operator is constructed. The Hartree-Fock equations are then solved by diagonalizing the Fock operator to obtain a new set of molecular orbitals and their corresponding energies. This new set of orbitals is compared to the previous set. If the change is below a predefined threshold, the procedure is considered converged, and the SCF is achieved. If convergence is not reached, the new set of orbitals is used to construct a new Fock operator, and the process is repeated. Convergence signifies that a stable electronic configuration has been reached within the limitations of the Hartree-Fock approximation.

In practical Hartree-Fock calculations, the spinorbitals are expressed as linear combinations of predefined mathematical functions known as basis functions. The set of these functions is called a basis set. Because a finite basis set cannot exactly represent the spinorbitals, they greatly define the level of accuracy

and computational cost of the calculation. Larger basis sets generally lead to more accurate descriptions of the electronic structure at the cost of increased computational effort.

2.1.1 Electron Correlation

The Hartree-Fock (HF) method is inherently limited by its neglect of the instantaneous interactions of electrons. In the HF approximation, each electron is treated as moving independently within a static, average field created by the other electrons. This mean-field approach fails to account for the fact that electrons will instantaneously repel each other, leading to a correlated movements as they try to avoid each other in space.
The primary consequence of neglecting electron correlation in the HF approximation is an overestimation of the electron-electron repulsion energy. While the HF method does account for the exchange interaction exactly as a consequence of the antisymmetry of the Slater determinant (Fermi correlation), it completely neglects the Coulomb, or dynamic, correlation. This omission leads to a higher electronic energy than the exact solution, and an inability to accurately predict certain phenomena, such as London dispersion forces.
The difference between the exact non-relativistic energy of the system and the energy obtained in the HF complete basis limit is defined as the correlation energy and is always negative due to the variational principle. Correlated methods aim to include the effects of the instantaneous interactions between electrons that are neglected in the mean-field approximation of HF theory. In the following sections, several correlated methods relevant to this work are presented.

2.1.2 Møller-Plesset Perturbation Theory

Møller-Plesset (MP) perturbation theory offers a way to improve upon the HF energy by the use of Raylei-Schro perturbation theory: the electron correlation is treated as a perturbation to the HF Hamiltonian. The energy and wavefunction are then expanded as a series in terms of the perturbation strength. The first-order energy correction in MP theory is zero, so the first non-trivial correction to the HF energy appears at the second order, giving rise to the MP2 method. The MP2 energy correction for a closed-shell molecule is given by:

$$E_{\mathrm{MP2}} = -\frac{1}{4}\sum_{ij}^{\mathrm{occ}}\sum_{ab}^{\mathrm{virt}}\frac{|\langle ij||ab\rangle|^2}{\epsilon_a + \epsilon_b - \epsilon_i - \epsilon_j} \tag{2.4}$$

Where i, j denote occupied molecular orbitals, a, b denote virtual molecular orbitals, and ϵ are the corresponding orbital energies from the HF calculation. MP theory can be extended to higher orders (MP3, MP4, etc.) to achieve greater accuracy, although the computational cost increases significantly with each order. The computational cost of MP2 scales as $O(N^5)$.

2.1.3 Density Functional Theory

Density Functional Theory (DFT) provides an alternative approach to incorporating electron correlation by parametrizing the energy on the electron density rather than the wavefunction, reducing the degrees of freedom of the system from $3N - 3$ to just 3. In the most commonly used form of DFT, the Kohn-Sham method, the prpblem is formulated terms of orbitals that are not physical, but are chosen to reproduce the electron density of the system. The fundamental principle of DFT is that the ground state energy of a system is a unique functional of its electron density:

$$\left(-\frac{1}{2}\nabla^2 + \hat{V}_{\text{ext}}(\mathbf{r}) + \hat{V}_{\text{H}}(\mathbf{r}) + \hat{V}_{\text{XC}}[\rho(\mathbf{r})]\right)\psi_i(\mathbf{r}) = \epsilon_i\psi_i(\mathbf{r}) \tag{2.5}$$

Where $\hat{V}_{\text{ext}}$ respresents the external potential, $\hat{V}_{\text{H}}(\mathbf{r}) = \int \frac{\rho(\mathbf{r}')}{|\mathbf{r}-\mathbf{r}'|}d\mathbf{r}'$ is the Hartree potential, $\hat{V}_{\text{XC}}$ is the Exchange-Correlation potential and $\rho(\mathbf{r})$ is the electron density. The exchange-correlation functional is the most challenging part of DFT, as it is not known exactly and must be approximated. The accuracy of DFT calculations depends heavily on the choice of exchange-correlation functional. The computational cost of DFT scales as $O(N^4)$.

2.1.4 Configuration Interaction

Configuration Interaction (CI) methods improve upon HF by expressing the electronic wavefunction as a linear combination of the HF ground state determinant and excited state determinants:

$$|\Psi_{\text{CI}}\rangle = c_0|\Phi_0\rangle + \sum_{ia} c_{ia}|\Phi_{ia}\rangle + \sum_{ijab} c_{ijab}|\Phi_{ijab}\rangle + \dots \tag{2.6}$$

Where $|\Phi_0\rangle$ is the HF ground state determinant, $|\Phi_{ia}\rangle$ represents a determinant with a hole in spin-orbital i and a particle in the spin-orbital a, and c are the CI coefficients. Full CI (FCI), includes all possible excitations within a given one-electron basis set and represents the exact solution to the non-relativistic Schrödinger equation in that basis. However, is computationally prohibitive

for all but the simplest systems. Full Configuration Interaction (FCI) includes all possible excitations within a given one-electron basis set and represents the exact solution to the non-relativistic Schrödinger equation in that basis. However, it is computationally prohibitive for all but the simplest systems.
Truncated CI methods, such as CISD (singles and doubles), are more practical but lack size extensivity —a property ensuring that the energy of a system scales correctly with the number of non-interacting subsystems. A method is size-extensive if, for two infinitely separated molecules A and B, the total energy satisfies $E(A+B) = E(A) + E(B)$. Truncated CI methods fail to satisfy this condition because they do not include all necessary higher-order excitations, leading to an underestimation of the total energy as system size grows.
CI are, however, size-consistent, meaning that the energy behaviour remains consistent when interaction between the involved molecular subsystems is nullified (by distance, for instance). While CISD is size-consistent, its lack of size extensivity makes it unsuitable for extensive systems.

2.1.5 Coupled Cluster Theory

Similarly to CI, the coupled cluster CC method expands the wavefunction as a linear combination of Slater determinats. However, the CC wavefunction is size-extensive and size-consistent by using an exponential ansatz,

$$|\Psi_{\mathrm{CC}}\rangle = e^{\hat{T}}|\Psi_0\rangle \tag{2.7}$$

where $\hat{T}$ is the cluster operator, which is the central component of CC theory and is defined as a sum of excitation operators,

$$\hat{T} = \hat{T}_1 + \hat{T}_2 + \hat{T}_3 + \cdots + \hat{T}_N \tag{2.8}$$

where N is the total number of electrons in the system. Each term in this sum corresponds to a specific level of excitation and is expressed within the second quantization formalism:

- $\hat{T}_1 = \sum_i^{\mathrm{occ}} \sum_a^{\mathrm{virt}} t_i^a a_a^\dagger a_i$ represents single excitations.
- $\hat{T}_2 = \frac{1}{4} \sum_{i,j}^{\mathrm{occ}} \sum_{a,b}^{\mathrm{virt}} t_{ij}^{ab} a_a^\dagger a_b^\dagger a_j a_i$ represents double, *coupled* excitations.
- Higher-order excitation operators $\hat{T}_3, \hat{T}_4, \ldots$ describe coupled excitation of three, four, and more electrons, respectively.

The coefficients t_i^a, t_{ij}^{ab}, etc., are cluster amplitudes to determined by projection of the CC Schrödinger equation onto the excited determinant. The exponential

form, expanded as a Taylor series,

$$e^{\hat{T}} = 1 + \hat{T} + \frac{1}{2!}\hat{T}^2 + \dots \tag{2.9}$$

inherently includes terms that represent disconnected clusters, which are ensures for size consistency. The energy is obtained by projecting onto the HF reference determinant:

$$E_{\text{CC}} = \langle \Psi_0 | e^{-\hat{T}} \hat{H} e^{\hat{T}} | \Psi_0 \rangle \tag{2.10}$$

Using the Baker-Campbell-Hausdorff expansion, the exponential operators in Eq. 2.10 can be simplified to a series of commutators which ends at the fourth order. The cluster operator $\hat{T}$ can be truncated at different levels of excitation:

- **CCD** (Coupled Cluster Doubles): This is the simplest approximation in the CC family, where the cluster operator is truncated to include only double excitations: $\hat{T} \approx \hat{T}_2$. There is no CC Singles since the Brilluin's theorem implies that the amplitudes of single excitations alone are null.
- **CCSD** (Coupled Cluster Singles and Doubles): This is one of the most widely used and generally accurate *ab initio* methods, where the cluster operator includes both single and double excitations: $\hat{T} \approx \hat{T}_1 + \hat{T}_2$.
- **CCSDT** (Coupled Cluster Singles, Doubles, and Triples): $\hat{T} \approx \hat{T}_1 + \hat{T}_2 + \hat{T}_3$.
- ...

The hierarchy can be extended to include even higher levels of excitation, with the properties converging to the FCI limit. The computational cost of CC methods increases rapidly with the level of truncation, as shown in Table 2.1.

Method	Operation count	Memory
HF	$O(N^4)$	$O(N^4)$
DFT	$O(N^4)$	$O(N^4)$
MP2	$O(N^5)$	$O(N^4)$
CCD/CCSD	$O(N^6)$	$O(N^4)$
CCSDT	$O(N^8)$	$O(N^6)$
CC2	$O(N^5)$	$O(N^4)$

Table 2.1: Computational scaling of quantum chemistry methods.

2.1.6 Second Approximate Coupled Cluster

Second Approximate Coupled Cluster (CC2) belongs to the broader family of CCn approximate coupled cluster methods, where the 'n' in CCn indicates the truncation of the cluster operator within a perturbative hierarchy. These methods aim to reduce the computational cost associated with standard CC truncations while still retaining a reasonable level of accuracy.

In CC2, the equations for the single amplitudes, t_i^a, are the same as CC theory (Eq. 2.7) under the constraint that the doubles amplitudes, t_{ij}^{ab}, are calculated using the non-iterative expression for MP2 (Eq 2.4). The resulting expression for the CC2 correlation energy is:

$$E_{\mathrm{CC2}} = \frac{1}{4}\sum_{ij}^{\mathrm{occ}}\sum_{ab}^{\mathrm{virt}}\frac{|\langle ij||ab\rangle|^2}{\epsilon_a + \epsilon_b - \epsilon_i - \epsilon_j} + \sum_{i}^{\mathrm{occ}}\sum_{a}^{\mathrm{virt}}\hat{F}_{ai}t_i^a \tag{2.11}$$

The perturbative treatment of the doubles amplitudes in CC2, reduces the computational cost compared to CCSD, Table 2.1. While this approximation can lead to a less accurate description of electron correlation, the inclusion of singles amplitudes allows for an approximate description of orbital relaxation, which often leads to higher quality wavefunction, and hence properties, compared to MP2.

2.2 Equation-of-Motion Methods

Equation-of-Motion Coupled Cluster (EOM-CC) methods are an extension of ground-state coupled cluster theory which provide a framework for calculating a variety of excited (EE), ionized (IP) and electron-attached (EA) states. In the EOM-CC, the target electronic state is generated by applying a linear excitation operator $\hat{R}$ to a reference state, which typically is the coupled cluster wavefunction of the ground state. The target state wavefunction can then be expressed as $|\Psi_{\mathrm{EOM}}\rangle = \hat{R}|\Psi_{\mathrm{CC}}\rangle = \hat{R}e^{\hat{T}}|\Phi_{\mathrm{HF}}\rangle$. Figure 2.1, shows some of the determinats of $|\Psi_{\mathrm{EA}}\rangle$, where the target state has one more α electron.

The form of the operator $\hat{R}$ is similar to the cluster operator and chosen to access the desired target state. In the case of EOM-EA, the electron attachment operator R^{EA} includes terms that describe the creation of one electron to an unoccupied orbital, terms that describe the creation of one electron accompanied by the excitation of another electron from an occupied to an unoccupied orbital,

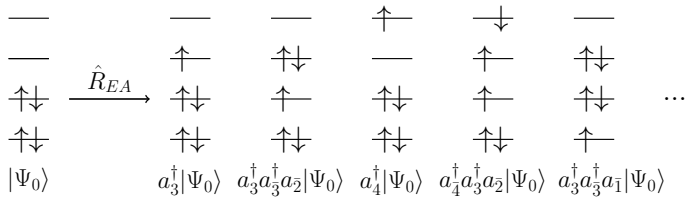

Figure 2.1: EOM-EA.

and so on:

$$\hat{R}^{\mathrm{EA}} = \hat{R}_1^{\mathrm{EA}} + \hat{R}_2^{\mathrm{EA}} + \ldots = \sum_a r^a a_a^\dagger + \frac{1}{2}\sum_{ab}\sum_i r_i^{ba} a_b^\dagger a_a^\dagger a_i + \ldots \tag{2.12}$$

Where a and b denote virtual orbitals, i denotes an occupied orbital, and r^a and r_i^{ba} are the coefficients to be determined. By truncating at the same excitation level as the cluster operator, the method is rigorously size-extensive and size-consistent. The EA energies, or any other EOM energy, can be obtained as the eigenvalues of the similarity-transformed Hamiltonian, $\bar{H}_{\mathrm{N}}$:

$$\bar{H}_{\mathrm{N}}\hat{R}|\Psi_0\rangle = \Delta E_{\mathrm{EOM}}\hat{R}|\Psi_0\rangle \tag{2.13}$$

$$\bar{H}_{\mathrm{N}} = e^{-\hat{T}}\hat{H}e^{\hat{T}} - \langle\Psi_0|e^{-\hat{T}}\hat{H}e^{\hat{T}}|\Psi_0\rangle \tag{2.14}$$

Since the similarity trnasformed hamiltonian is non-hermitian, the left and right are different but correspond to the same eigenvalues. This means that the properties have 'right' and 'left' expectation values.
The strength of the EOM-CC ansatz is the use of a closed shell reference to access open shell states, which are eigenfunctions of the $\hat{S}^2$ operator. The EOM-CC methods are also size-extensive and size-consistent. The computational cost of EOM-CC methods is similar to that of the corresponding ground-state CC methods.

2.3 Dyson Orbitals

Dyson orbitals are defined as the overlap between the wavefunction of an initial N-electron state ($|\Psi_0^N\rangle$) and the wavefunction of the final state with $N \pm 1$ electrons ($|\Psi_f^{N\pm1}\rangle$).

$$\phi_d(r_1) = \sqrt{N}\int \Psi^N(r_2,\ldots,r_N)\Psi^{N+1}(r_1,r_2,\ldots,r_N)\,dr_2\ldots dr_N \tag{2.15}$$

Because the the terms differ in one electron, the result of the overlap is a vector instead of a scalar, and can be expressed as a linear combination of the molecular orbitals ($\phi_p(r)$) of the reference wavefunction:

$$\phi_d(r) = \sum_p \gamma_p \phi_p(r) \tag{2.16}$$

where γ_p are the coefficients that quantify the contribution of each molecular orbital to the Dyson orbital. Physically, Dyson orbitals can be interpreted as the correlated analog to the orbital of the electron that is either removed or attached.

The norm squared of the Dyson orbital, (P), is calculated by integrating the squared modulus of the Dyson orbital over all space:

$$P = \int |\phi_{Dyson}(r)|^2 \, dr = \sum_{p,q} \gamma_p^* \gamma_q \langle \phi_p | \phi_q \rangle \tag{2.17}$$

The pole strength ranges from 0 to 1 and provides a direct measure of the one-electron character of the ionization or electron attachment process. As the open shell wavefunction is usually obtained by means of a EOM-CC method, there are a 'left' and 'right' Dyson orbital.

They can be used for the interpretation and prediction of photoelectron spectra as they contain all the information required to calculate diffrential corss-sections, $\frac{d\sigma}{d\Omega_k}$:

$$\frac{d\sigma}{d\Omega_k} = \frac{4\pi^2 k E}{c} |\langle \phi_d | \mu | \Psi_k^{el} \rangle|^2 \tag{2.18}$$

where where k is the magnitude of the photoelectron wavevector, E is the energy of the ionizing radiation, and c is the speed of light, μ is the dipole operator, and Ψ_k^{el} is the photoelectron wavefunction, and a strong orthonormality is assumed between the reference and continuum wavefunction.

2.3.1 EOM-CC2 Dyson Orbital Equations

Computes O block of matrix elements of dyson orbitals using CC and EOM-EA wave functions:

$$\langle EA|a|EE\rangle = \langle 0|L^{EE}(ae^T)_c R^{EA}|0\rangle$$

The storage convention assumed for the r2 IP amplitudes is:

$$r2^a_{ij} a^\dagger ji - - - r2(i|j|a)$$

The storage convention assumed for the l2 IP amplitudes is

$$l2^{a}_{ij} i^\dagger j^\dagger a --- l2(i|j|a)$$

EOM-EA-Dyson Equations

A derivation of the dyson equation in terms of the t, r, l, λ amplitudes is presented. It is importnat to realize that the operators involved $(\hat{T}, \hat{\Lambda}, \hat{R}, \hat{L})$ affect the occupation of the spin-orbitals, and thus only the combinations of terms which leave the refrence wavefunction, $|0\rangle$, unchanged survive. To find these combinations, commutators can be used to reorder the operators involved:

In the case of the right EOM-EA-Dyson orbital amplitudes:

$$\gamma_i^{\mathrm{EA,R}} = \langle EA|\hat{a}_i^\dagger|CC\rangle = \langle 0|\hat{L}^{EA} e^{-\hat{T}} \hat{a}_i^\dagger e^{\hat{T}}|0\rangle$$

The following equalities are usueful:

$$e^{-\hat{T}} e^{\hat{T}} = e^{\hat{T}} e^{-\hat{T}} = 1$$

$$[e^{\pm\hat{T}}, \hat{a}_p^\dagger] = \cancelto{0}{[1, \hat{p}^\dagger]} \pm t_j^b [\hat{b}^\dagger \hat{j}, \hat{p}^\dagger] \pm t_{jk}^{bc} [\hat{b}^\dagger \hat{c}^\dagger \hat{k} \hat{j}, \hat{p}^\dagger] + \dots$$

Where a change of notation, $a_p^\dagger \to p^\dagger$, upon expansion is done for readibility. Two cases are distinguished, p is a virtual orbital, a, or an occupied orbital, i. For virtual orbitals, $p = a$:

$$[\hat{b}^\dagger \hat{j}, \hat{a}^\dagger] = \hat{b}^\dagger \hat{j} \hat{a}^\dagger - \hat{a}^\dagger \hat{b}^\dagger \hat{j} = (-1)^2 \hat{a}^\dagger \hat{b}^\dagger \hat{j} - \hat{a}^\dagger \hat{b}^\dagger \hat{j} = 0$$

Similarly with higher order terms, it is arribed to:

$$[e^{\pm\hat{T}}, \hat{a}_a^\dagger] = 0$$

For occupied orbitals, $p = i$:

$$[\hat{b}^\dagger \hat{j}, \hat{i}^\dagger] = \hat{b}^\dagger \hat{j} \cancelto{0}{\hat{i}^\dagger} - \hat{i}^\dagger \hat{b}^\dagger \hat{j}$$

And similarly with higher order terms:

$$[e^{\pm\hat{T}}, \hat{a}_i^\dagger] = -\hat{a}_i^\dagger (e^{\pm\hat{T}} - 1)$$

These relations can now be used to derive the expression for the occupied and virtual Right EOM-EA-Dyson orbital amplitudes:

$$\phi_{\mathrm{D}}^{\mathrm{EA,R}} = \sum_p \gamma_p^{\mathrm{EA,R}} \phi_p = \sum_i^{\mathrm{occ}} \gamma_i^{\mathrm{EA,R}} \phi_i + \sum_a^{\mathrm{vir}} \gamma_a^{\mathrm{EA,R}} \phi_a$$

The general expression can be reordered:

$$\begin{aligned}\gamma_p^{\mathrm{EA,R}} &= \langle EA|\hat{a}_p^\dagger|CC\rangle = \langle 0|\hat{L}^{EA}e^{-\hat{T}}\hat{a}_p^\dagger e^{\hat{T}}|0\rangle \\ &= \langle 0|\hat{L}^{EA}(\hat{a}_p^\dagger e^{-\hat{T}} + [e^{-\hat{T}}, \hat{a}_p^\dagger])e^{\hat{T}}|0\rangle \end{aligned} \tag{2.19}$$

For virtual orbitals, $p = a$:

$$\begin{aligned}\gamma_a^{\mathrm{EA,R}} &= \langle 0|\hat{L}^{EA}(\hat{a}_a^\dagger e^{-\hat{T}} + \cancelto{0}{[e^{-\hat{T}}, \hat{a}_a^\dagger]})e^{\hat{T}}|0\rangle \\ &= \langle 0|\hat{L}^{EA}\hat{a}_a^\dagger \cancelto{1}{e^{-\hat{T}}e^{\hat{T}}}|0\rangle = \langle 0|\hat{L}^{EA}\hat{a}_a^\dagger|0\rangle \\ &= \langle 0|l_a\hat{a}\hat{a}^\dagger|0\rangle \\ &= l_a \end{aligned} \tag{2.20}$$

For occupied orbitals, $p = i$:

$$\begin{aligned}\gamma_i^{\mathrm{EA,R}} &= \langle 0|\hat{L}^{EA}(\hat{a}_i^\dagger e^{-\hat{T}} + [e^{-\hat{T}}, \hat{a}_i^\dagger])e^{\hat{T}}|0\rangle \\ &= \langle 0|\hat{L}^{EA}(\cancelto{0}{\hat{a}_i^\dagger e^{-\hat{T}}} - \hat{a}_i^\dagger e^{-\hat{T}} + \hat{a}^\dagger)e^{\hat{T}}|0\rangle = \langle 0|\hat{L}^{EA}\hat{a}_i^\dagger e^{\hat{T}}|0\rangle \\ &= \langle 0|l_b t_i^b\,\hat{b}\hat{i}^\dagger\hat{b}^\dagger\hat{i} + l_{bc}^j t_{ij}^{bc}\,\hat{b}\hat{c}\hat{j}^\dagger\hat{i}^\dagger\hat{b}^\dagger\hat{c}^\dagger\hat{i}\hat{j}|0\rangle \\ &= -\sum_c t_{ic}l_c - \frac{1}{2}\sum_{kcd} t_{ki}^{dc}l_{dc}^k \end{aligned} \tag{2.21}$$

A similar approach can be applyed to the other Dyson equations to obtain the expressions.

Left EOM-EA-Dyson orbital, $\phi_{\mathrm{D}}^{\mathrm{EA,L}} = \sum_i^{\mathrm{occ}} \gamma_i^{\mathrm{EA,L}}\phi_i + \sum_a^{\mathrm{vir}} \gamma_a^{\mathrm{EA,L}}\phi_a$:

$$\begin{aligned}\gamma_i^{\mathrm{EA,L}} &= \langle CC|\hat{a}_i|EA\rangle \\ &= -\sum_c \lambda_{ic}r_c - \frac{1}{2}\sum_{kcd}\lambda_{ik}^{cd}r_k^{dc} \end{aligned} \tag{2.22}$$

$$\begin{aligned}\gamma_a^{\mathrm{EA,L}} &= \langle CC|\hat{a}_a|EA\rangle \\ &= r_a + \sum_{kc}\lambda_{kc}r_{ca}^k + \sum_k \gamma_k^{\mathrm{EA,L}}t_{ka} - \frac{1}{2}\sum_{klcd}\lambda_{lk}^{dc}t_{lk}^{da}r_c \end{aligned} \tag{2.23}$$

EOM-EA-EE-Dyson Equations

Right Dyson orbital, $\phi_{\mathrm{D}}^{\mathrm{EA-EE,R}} = \sum_i^{\mathrm{occ}} \gamma_i^{\mathrm{EA-EE,R}} \phi_i + \sum_a^{\mathrm{vir}} \gamma_a^{\mathrm{EA-EE,R}} \phi_a$:

$$\begin{aligned}\gamma_i^{\mathrm{EA-EE,R}} &= \langle EA|\hat{a}_i^\dagger|EE\rangle \\ &= r_0 \gamma_a^{\mathrm{EA,R}} - \sum_c r_{ic} l_c - \frac{1}{2}\sum_{lcd} r_{il}^{cd} l_{dc}^{l} - \sum_{lcd} l_{dc}^{l} t_{ic} r_{ld} \end{aligned} \tag{2.24}$$

$$\begin{aligned}\gamma_a^{\mathrm{EE-EA,R}} &= \langle EA|\hat{a}_a^\dagger|EE\rangle \\ &= r_0 l_a + \sum_{kc} l_{ca}^{k} r_{kc} \end{aligned} \tag{2.25}$$

Left Dyson orbital, $\phi_{\mathrm{D}}^{\mathrm{EE-EA,L}} = \sum_i^{\mathrm{occ}} \gamma_i^{\mathrm{EE-EA,L}} \phi_i + \sum_a^{\mathrm{vir}} \gamma_a^{\mathrm{EE-EA,L}} \phi_a$:

$$\begin{aligned}\gamma_i^{\mathrm{EE-EA,L}} &= \langle EE|\hat{a}_i|EA\rangle \\ &= -\sum_c l_{ic} r_c - \frac{1}{2}\sum_{kcd} l_{ik}^{cd} r_k^{dc} \end{aligned} \tag{2.26}$$

$$\begin{aligned}\gamma_a^{\mathrm{EE-EA,L}} &= \langle EE|\hat{a}_a|EA\rangle \\ &= \sum_{kc} l_{kc} r_{ca}^{k} + \sum_k \gamma_k^{\mathrm{EE-EA,L}} t_{ka} - \frac{1}{2}\sum_{klcd} l_{lk}^{dc} t_{lk}^{da} r_c \end{aligned} \tag{2.27}$$

EOM-IP-Dyson Equations

Right Dyson orbital, $\phi_{\mathrm{D}}^{\mathrm{EE,R}} = \sum_i^{\mathrm{occ}} \gamma_i^{\mathrm{IP,R}} \phi_i + \sum_a^{\mathrm{vir}} \gamma_a^{\mathrm{IP,R}} \phi_a$:

$$\begin{aligned}\gamma_a^{\mathrm{IP,R}} &= \langle CC|\hat{a}_a^\dagger|IP\rangle \\ &= \lambda_{ka} r_k + \frac{1}{2}\lambda_{lk}^{ca} r_{klc} \end{aligned} \tag{2.28}$$

$$\begin{aligned}\gamma_i^{\mathrm{IP,R}} &= \langle CC|\hat{a}_i^\dagger|IP\rangle \\ &= r_i + \sum_{kc} \lambda_{kc} r_{ik}^{c} - \sum_c \gamma_c^{\mathrm{IP,R}} t_{ic} - \frac{1}{2}\sum_{klcd} \lambda_{lk}^{dc} t_{li}^{dc} r_k \end{aligned} \tag{2.29}$$

Left Dyson orbital, $\phi_{\mathrm{D}}^{\mathrm{IP,L}} = \sum_i^{\mathrm{occ}} \gamma_i^{\mathrm{IP,L}} \phi_i + \sum_a^{\mathrm{vir}} \gamma_a^{\mathrm{IP,L}} \phi_a$:

$$\begin{aligned}\gamma_i^{\mathrm{IP,L}} &= \langle IP|\hat{a}_i|CC\rangle \\ &= l_i \end{aligned} \tag{2.30}$$

$$\begin{aligned}\gamma_a^{\mathrm{IP,L}} &= \langle IP|\hat{a}_a|CC\rangle \\ &= \sum_k t_{ka} l_k + \frac{1}{2}\sum_{klc} t_{kl}^{ac} l_{kl}^{c} \end{aligned} \tag{2.31}$$

EOM-EE-IP-Dyson Equations

Right Dyson orbital, $\phi_{\mathrm{D}}^{\mathrm{EE-IP,R}} = \sum_i^{\mathrm{occ}} \gamma_i^{\mathrm{EE-IP,R}} \phi_i + \sum_a^{\mathrm{vir}} \gamma_a^{\mathrm{EE-IP,R}} \phi_a$:

$$\begin{aligned}\gamma_i^{\mathrm{EE-IP,R}} &= \langle EE|\hat{a}_i^\dagger|IP\rangle \\ &= \sum_{kc} l_{kc} r_{ik}^{c} - \sum_c \gamma_c^{IP-EI} t_{ic} - \frac{1}{2}\sum_{klcd} l_{lk}^{dc} t_{li}^{dc} r_k \end{aligned} \tag{2.32}$$

$$\begin{aligned}\gamma_a^{\mathrm{EE-IP,R}} &= \langle EE|\hat{a}_a^\dagger|IP\rangle \\ &= l_{ka} r_k + \frac{1}{2} l_{lk}^{ca} r_{klc} \end{aligned} \tag{2.33}$$

Left Dyson orbital, $\phi_{\mathrm{D}}^{\mathrm{IP-EE,L}} = \sum_i^{\mathrm{occ}} \gamma_i^{\mathrm{IP-EE,L}} \phi_i + \sum_a^{\mathrm{vir}} \gamma_a^{\mathrm{IP-EE,L}} \phi_a$:

$$\begin{aligned}\gamma_i^{\mathrm{IP-EE,L}} &= \langle IP|\hat{a}_i|EE\rangle \\ &= r_0 l_i + \sum_{kc} l_{ik}^{c} r_{kc} \end{aligned} \tag{2.34}$$

$$\begin{aligned}\gamma_a^{\mathrm{IP-EE,L}} &= \langle IP|\hat{a}_a|EE\rangle \\ &= r_0 \gamma_a^{\mathrm{IP,L}} + \sum_k r_{ka} l_k + \frac{1}{2}\sum_{klc} r_{kl}^{ac} l_{kl}^{c} + \sum_{klc} l_{kl}^{c} t_{ka} r_{cl} \end{aligned} \tag{2.35}$$

Chapter 3

Computational Methods

All electronic structure calculations were performed using the developer's copy of the *QChem* software [2]. In all computations the frozen-core approximation is used, only the valence orbitals are correlated, as well as the resolution of the identity (RI) approximation, auxiliary basis functions are used to approximate the Coulumb operator integrals, reducing its scaling to $N(O^3)$ [5].

For the EOM-EA calculations, the reference wavefunction was obtained as the restricted Hartree-Fock (RHF) solution of the ground state of the neutral molecule. Unless explecitly mention, calculations were performed at using the aug-cc-pVDZ basis set [1] further augmented by 3 s-shells on hydrogen atoms and 6 s- and 3 p-shells on all non-hydrogen atoms [7] to properly model the non-valence states. The coefficients of the extra functions were obtained by halving the most diffuse function of the original set.

Photoionization and Photodetachment crossections were calculated using the *ezDyson* package [4, 3].

Chapter 4

Results and Discussion

4.1 Performance of EOM-CC2 Related Methods

...

4.1.1 Basis Set Dependence of EA-EOM-CC2 in Dipole Bound Anions

...

		RI-CC2						RI-CCSD			
			aug-cc-pVTZ			pVDZ	pVQZ	pVDZ	pTDZ		
Molecule		2s1p	4s2p	6s3p	8s4p	6s3p	6s3p	6s3p	6s3p	KT	μ(D)
Acetaldehyde	CH_3CHO	-156.7	-27.8	-3.2	0.8	-4.6	-3.2	-4.6	-3.1	-0.428	3.29
Acetone	$(CH_3)_2CO$	-114.9	-16.8	1.3	3.3	-0.3	0.9	-0.5	0.9	-5.1	3.46
Acetonitrile	CH_3CN	-61.2	12.6	19.9	20.1	18.2	20.3	17.1	18.4	4.2	4.29
Benzaldehyde	C_6H_5CHO	-97.1	-2.1	8.9	9.6	7.4	9.1	3.4	4.6	-4.9	3.77
N,N-Dimethylformamide	$(CH_3)_2NCHO$	-81.1	5.4	14.1	14.4	13.2	14.4	13.3	13.7	1.9	4.48
DMSO	$(CH_3)_2SO$	-84.5	4.0	15.4	16.1	14.8	15.5	14.7	14.9	2.1	4.63
Formamide	CH_3NO	-92.2	1.1	16.2	17.2	15.1	17.0	15.1	15.9	3.4	4.28
Methylisocyanide	CH_3NC	-95.1	-0.5	10.0	10.5	9.5	10.1	8.8	9.0	-1.8	3.59
Nitrobenzene	$C_6H_5NO_2$	-63.6	30.6	34.8	34.8	32.5	-	25.0	25.9	5.4	5.15
Nitromethane	CH_3NO_2	-82.9	5.7	14.2	14.7	13.0	14.7	12.9	13.7	3.5	4.10
Nitrosobenzene	C_6H_5NO	-125.0	1.0	11.4	-	9.9	-	5.1	6.0	-4.1	3.73
Phenylisocyanide	C_6H_5NC	-82.7	8.6	16.3	16.5	15.2	16.7	9.0	9.2	-4.9	3.61
Pyridazine	$C_4H_4N_2$	-80.7	20.5	26.3	26.4	25.0	26.7	18.6	19.1	1.7	4.41
Vinylene carbonate	$C_3H_2O_3$	-82.5	20.9	27.2	27.4	26.4	27.7	25.1	25.5	10	5.05
	MAE	105.3	8.8	2.8	3.4	2.3	2.4	0.8	ref.		

Table 4.1: EOM-EA binding energies of dipole-bound radical anions computed using different augmented Dunning basis sets and RI-CC2 and RI-CCSD for the the test set of moluces [7]. A positive value corresponds to a bound electron. Koopmans' theorem (KT), and dipole momment (μ), calculated at the HF level, and mean absolute error (MAE) are also given. The values are in meV and D respectively.

4.1.2 Performance of EA-EOM-CC2 on Valence Bound Radical Anion States of Quinones

Mol.	Ref. [8] Exp (aEA)	Ref. [8] CCSD(T) +E_{CBS}	RI-CC2 No SCS	RI-CC2 SCS
1	1.91	1.64	2.02	1.54
2	1.85	1.57	1.95	-
3	1.76	1.49	1.89	1.39
4	1.77	1.5	1.89	1.40
5	1.69	1.43	1.84	1.34
6	1.62	1.42	1.83	1.32
7	1.72	1.32	1.65	1.17
8	1.86	1.5	1.88	1.39
9	1.81	1.55	1.97	-
10	1.74	1.51	1.92	1.45

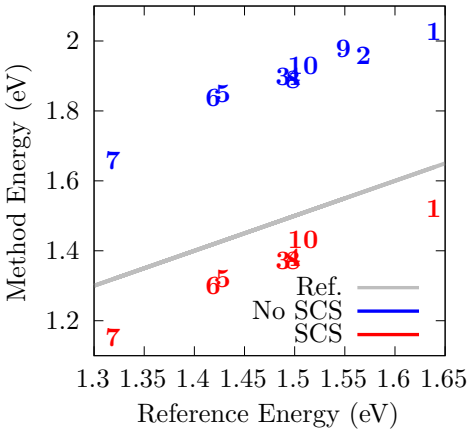

Table 4.2 and **Figure 4.1:** Comparison between reference and RI-CC2 data for quinones. The table also includes the experimental value (adiabatic EA instead of veritacl EA).

SCS improves the result for valence state of CC2, whihc is in accordance with the conclusions from [7]. Something to note is that when comparing the results with experiments, one can think that CC2 gets close than CCSD. This however, can be explained by the fact that the experiment measures the adiabatic electron binding energy, while the calculations are performed for the vertical EA. As the former energy ...

4.1.3 Photoelectron Cross-section Calculations from EOM-CC2/CCSD

...

4.2 Study on the Anion States of Ubiquinone

...

4.2.1 Energy and Dipole Surfaces of CoQ

...

Q0

a

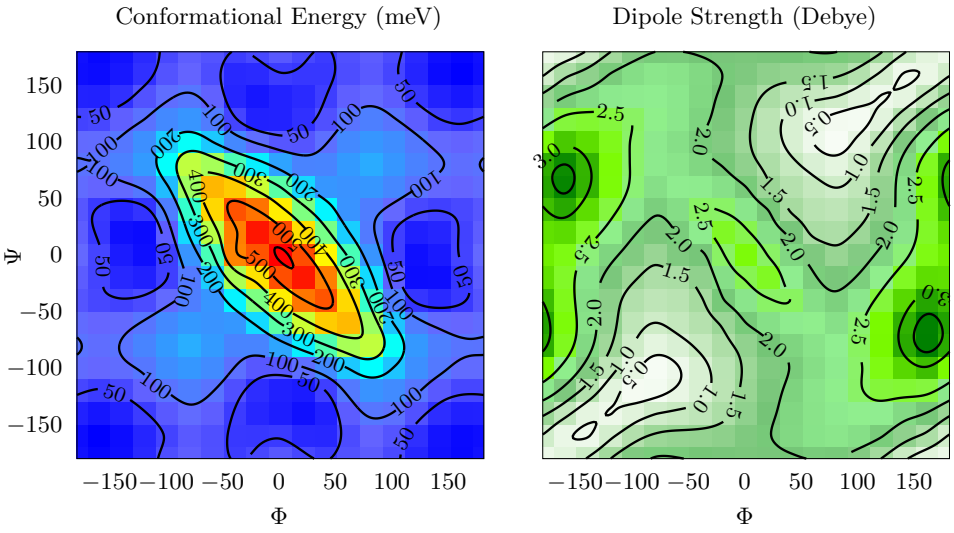

Figure 4.2: Surfaces of Q0. Left: Energy surface. Right: Dipole moment surface.

...

Q1

...

4.2.2 A Simple Cluster Model

...

4.2.3 Interaction with Water

...

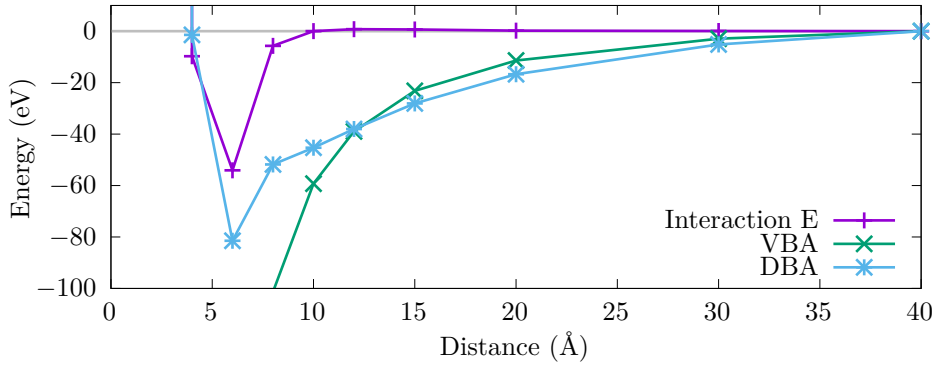

Figure 4.3: Favorable Interaction with water.

4.2.4 Effect of Nearby Amionacids

...

Serine

...

Threonine

...

Apsaragine

...

Isoleucine

...

Chapter 5

This is conclusion

...

Instructions by the Arenberg Doctoral School:

An extensive conclusion, including a global discussion of the research results, a discussion of the implications of the PhD research and future perspectives in regards to follow-up research.

Appendix A

This is myappendix

...

Instructions by the Arenberg Doctoral School:

Appendices: The appendices should include parts of the research which are essential for the work, but which may hamper the readability of the text, e.g. because of their length (mathematical deductions, experimental data, examples, figures, etc.).

Bibliography

[1] Dunning Jr, T. H. Gaussian basis sets for use in correlated molecular calculations. i. the atoms boron through neon and hydrogen. *The Journal of chemical physics 90*, 2 (1989), 1007–1023.

[2] Epifanovsky, E., Gilbert, A. T. B., Feng, X., Lee, J., Mao, Y., Mardirossian, N., Pokhilko, P., White, A. F., Coons, M. P., Dempwolff, A. L., Gan, Z., Hait, D., Horn, P. R., Jacobson, L. D., Kaliman, I., Kussmann, J., Lange, A. W., Lao, K. U., Levine, D. S., Liu, J., McKenzie, S. C., Morrison, A. F., Nanda, K. D., Plasser, F., Rehn, D. R., Vidal, M. L., You, Z.-Q., Zhu, Y., Alam, B., Albrecht, B. J., Aldossary, A., Alguire, E., Andersen, J. H., Athavale, V., Barton, D., Begam, K., Behn, A., Bellonzi, N., Bernard, Y. A., Berquist, E. J., Burton, H. G. A., Carreras, A., Carter-Fenk, K., Chakraborty, R., Chien, A. D., Closser, K. D., Cofer-Shabica, V., Dasgupta, S., de Wergifosse, M., Deng, J., Diedenhofen, M., Do, H., Ehlert, S., Fang, P.-T., Fatehi, S., Feng, Q., Friedhoff, T., Gayvert, J., Ge, Q., Gidofalvi, G., Goldey, M., Gomes, J., González-Espinoza, C. E., Gulania, S., Gunina, A. O., Hanson-Heine, M. W. D., Harbach, P. H. P., Hauser, A., Herbst, M. F., Hernández Vera, M., Hodecker, M., Holden, Z. C., Houck, S., Huang, X., Hui, K., Huynh, B. C., Ivanov, M., Jász, Á., Ji, H., Jiang, H., Kaduk, B., Kähler, S., Khistyaev, K., Kim, J., Kis, G., Klunzinger, P., Koczor-Benda, Z., Koh, J. H., Kosenkov, D., Koulias, L., Kowalczyk, T., Krauter, C. M., Kue, K., Kunitsa, A., Kus, T., Ladjánszki, I., Landau, A., Lawler, K. V., Lefrancois, D., Lehtola, S., Li, R. R., Li, Y.-P., Liang, J., Liebenthal, M., Lin, H.-H., Lin, Y.-S., Liu, F., Liu, K.-Y., Loipersberger, M., Luenser, A., Manjanath, A., Manohar, P., Mansoor, E., Manzer, S. F., Mao, S.-P., Marenich, A. V., Markovich, T., Mason, S., Maurer, S. A., McLaughlin, P. F., Menger, M. F. S. J., Mewes, J.-M., Mewes, S. A., Morgante, P., Mullinax, J. W., Oosterbaan, K. J.,

Paran, G., Paul, A. C., Paul, S. K., Pavošević, F., Pei, Z., Prager, S., Proynov, E. I., Rák, Á., Ramos-Cordoba, E., Rana, B., Rask, A. E., Rettig, A., Richard, R. M., Rob, F., Rossomme, E., Scheele, T., Scheurer, M., Schneider, M., Sergueev, N., Sharada, S. M., Skomorowski, W., Small, D. W., Stein, C. J., Su, Y.-C., Sundstrom, E. J., Tao, Z., Thirman, J., Tornai, G. J., Tsuchimochi, T., Tubman, N. M., Veccham, S. P., Vydrov, O., Wenzel, J., Witte, J., Yamada, A., Yao, K., Yeganeh, S., Yost, S. R., Zech, A., Zhang, I. Y., Zhang, X., Zhang, Y., Zuev, D., Aspuru-Guzik, A., Bell, A. T., Besley, N. A., Bravaya, K. B., Brooks, B. R., Casanova, D., Chai, J.-D., Coriani, S., Cramer, C. J., Cserey, G., DePrince, A. E., DiStasio, R. A., Dreuw, A., Dunietz, B. D., Furlani, T. R., Goddard, W. A., Hammes-Schiffer, S., Head-Gordon, T., Hehre, W. J., Hsu, C.-P., Jagau, T.-C., Jung, Y., Klamt, A., Kong, J., Lambrecht, D. S., Liang, W., Mayhall, N. J., McCurdy, C. W., Neaton, J. B., Ochsenfeld, C., Parkhill, J. A., Peverati, R., Rassolov, V. A., Shao, Y., Slipchenko, L. V., Stauch, T., Steele, R. P., Subotnik, J. E., Thom, A. J. W., Tkatchenko, A., Truhlar, D. G., Van Voorhis, T., Wesolowski, T. A., Whaley, K. B., Woodcock, H. L., Zimmerman, P. M., Faraji, S., Gill, P. M. W., Head-Gordon, M., Herbert, J. M., and Krylov, A. I. Software for the frontiers of quantum chemistry: An overview of developments in the q-chem 5 package. *J. Chem. Phys. 155*, 8 (2021), 084801.

[3] Gozem, S., and Krylov, A. I. Photoionization and photodetachment spectra from equation-of-motion coupled-cluster dyson orbitals. *Chem. Lett 6* (2015), 4532–4540.

[4] Gozem, S., and Krylov, A. I. The ezspectra suite: An easy-to-use toolkit for spectroscopy modeling. *Wiley Interdisciplinary Reviews: Computational Molecular Science 12*, 2 (2022), e1546.

[5] Hättig, C., and Weigend, F. Cc2 excitation energy calculations on large molecules using the resolution of the identity approximation. *The Journal of Chemical Physics 113*, 13 (2000), 5154–5161.

[6] Jordan, K. D., and Wang, F. Theory of dipole-bound anions. *Annual review of physical chemistry 54*, 1 (2003), 367–396.

[7] Paran, G. P., Utku, C., and Jagau, T.-C. On the performance of second-order approximate coupled-cluster singles and doubles methods for non-valence anions. *Physical Chemistry Chemical Physics 26*, 3 (2024), 1809–1818.

[8] Schulz, C. E., Dutta, A. K., Izsák, R., and Pantazis, D. A. Systematic high-accuracy prediction of electron affinities for biological quinones. *Journal of Computational Chemistry 39*, 29 (2018), 2439–2451.

[9] Szabo, A., and Ostlund, N. S. *Modern quantum chemistry: introduction to advanced electronic structure theory*. Courier Corporation, 1996.

Statement on the use of Generative AI

Instructions by the Arenberg Doctoral School:

Read the guidelines in relation to GenAI at KU Leuven and add the ‘statement on the use of Generative AI’ in your manuscript.

Generative AI was used for lenguage and coding assistance (ChatGPT, MicrosoftCopilot, LeChat).
The text, code, and images in this thesis are my own (unless otherwise specified). Generative AI has only been used in accordance with the KU Leuven guidelines and appropriate references have been added. I have reviewed and edited the content as needed and I take full responsibility for the content of the thesis.

DEPARTMENT OF CHEMISTRY
DEPARTMENT OF CHEMISTRY
Celestijnenlaan 200A box 2402
B-3001 Leuven
first.name@dept.kuleuven.be
https://chem.kuleuven.be/en/research/qcpc/tue/